High efficiency grating couplers for strain tunable GaAs quantum dot based entangled photon sources 🕩

Constantin Schmidt ✉ 🆔 ; Chenxi Ma 🆔 ; Frederik Benthin 🆔 ; Jingzhong Yang 🆔 ; Eddy P. Rugeramigabo 🆔 ;
Michael Zopf ✉ 🆔 ; Fei Ding 🆔

Check for updates

View Online

Export Citation

CrossMark

High efficiency grating couplers for strain tunable GaAs quantum dot based entangled photon sources ⓕ

View Online Export Citation CrossMark

Constantin Schmidt,[1,a)] ⓘD Chenxi Ma,[1] ⓘD Frederik Benthin,[1] ⓘD Jingzhong Yang,[1] ⓘD
Eddy P. Rugeramigabo,[1] ⓘD Michael Zopf,[1,a)] ⓘD and Fei Ding[1,2,b)] ⓘD

AFFILIATIONS

[1] Institut für Festkörperphysik, Gottfried Wilhelm Leibniz Universität Hannover, Appelstr. 2, 30167 Hannover, Germany

[2] Laboratorium für Nano- und Quantenengineering, Gottfried Wilhelm Leibniz Universität Hannover, Schneiderberg 39, 30167 Hannover, Germany

a) Authors to whom correspondence should be addressed: constantin.schmidt@fkp.uni-hannover.de
and michael.zopf@fkp.uni-hannover.de
b) fei.ding@fkp.uni-hannover.de

ABSTRACT

The on-chip integration of single photon and entangled photon emitters such as epitaxially grown semiconductor quantum dots into photonic frameworks is a rapidly evolving research field. GaAs quantum dots offer high purity and a high degree of entanglement due to, in part, exhibiting very small fine structure splitting along with short radiative lifetimes. Integrating strain-tunable quantum dots into nanostructures enhances the quantum optical fingerprint, i.e., radiative lifetimes and coupling of these sources, and allows for on-chip manipulation and routing of the generated quantum states of light. Efficient out-coupling of photons for off-chip processing and detection requires carefully engineered mesoscopic structures. Here, we present numerical studies of highly efficient grating couplers reaching up to over 90% transmission. A 2D Gaussian mode overlap of 83.39% for enhanced out-coupling of light from within strain-tunable photonic nanostructures for free-space transmission and single-mode fiber coupling is shown. The photon wavelength under consideration is 780 nm, corresponding to the emission from GaAs quantum dots resembling the ^{87}Rb D$_2$ line. The presented numerical study helps implement such sources for applications in complex quantum optical networks.

I. INTRODUCTION

The rapid advancement of integrated photonic circuits is important toward realizing scalable platforms for quantum technologies. Notably, the interaction between photons and single entities of matter in solid state environments has firm implications for linear optical quantum computation,[1] quantum communication,[2–4] quantum metrology,[5] as well as the exploitation of nonlinear quantum optics.[6,7] At the heart of these envisioned quantum information applications lies the generation of single photons and entangled multi-photon states. Deterministic solid-state emitters encompass molecules,[8] color centers in diamonds,[9] and semiconductor quantum dots (QDs).[10–12] In particular,

semiconductor QDs have emerged as preeminent candidates for on-demand triggered single photon and entangled photon pair sources. They feature bright and pure emissions[13] with high entanglement fidelities near unity[14] using the biexciton–exciton cascade. Photons generated by epitaxial QDs stand out with high indistinguishability and immense rates due to the high dipole strengths of QDs.

GaAs QDs based on *in situ* droplet etching and nanohole infilling offer the advantage of lifetime-limited emission linewidths.[15] The stoichiometry of such QDs determines their emission wavelengths in the range of 700–800 nm, which can be adjusted during growth by controlling the infilling amount in the growth direction. Beyond the scope of this, GaAs QDs can be grown nearly strain-free, resulting in low variances in optical characteristics. Auspiciously,

the D_2 line of ^{87}Rb atoms (780 nm) coincides with this wavelength window. This line is commonly used for atom-based quantum memories for hybrid quantum networks.[16–18] GaAs/AlGaAs QDs exploit similar emission fingerprints, benefiting their coherent implementation into scalable integrated photonic circuits.[19] In order to fully compensate for their remaining spectral mismatch, tuning methods like Stark tuning[20] and strain tuning[21] can be employed. Remarkably, the strain tuning method further offers the possibility to control excitonic lifetimes, g-factors, and heavy/light-hole mixing while being compatible with on-chip setups.[22]

The semiconductor host features a high refractive index in contrast to the surrounding environment, giving rise to total internal reflection at the interface. On one hand, the large refractive index contrast allows for the realization of waveguiding nanostructures, which constitute key building blocks for complex quantum photonic frameworks. On the other hand, this is detrimental to the efficient collection of the emitted light. An approach to promote the scalability of quantum optical frameworks lies in the use of complex integrated waveguide circuits. For example, two QDs can be interfaced with waveguides, which are then spatially combined to form a 3 dB directional coupler. Establishing this approach would enable the demonstration of two-photon interference of distant quantum emitters with integrated individual strain tuning. Possible coupling schemes to collect the generated light involve, e.g., end-fire coupling from tapered waveguides to a cleaved interfacing single-mode optical fiber[23] as well as evanescent field coupling between a tapered waveguide section and a microfiber.[24] The latter coupling method has been experimentally demonstrated to reach around 6% collection efficiency in the case of interfaced InAs QDs, corresponding to a single photon rate of 3.0 MHz.[25] Albeit the enhanced photon yield, this comes at the expense of increased manufacturing and alignment complexity, forming the necessity for expensive cryostatic alignment systems. In order to circumvent this, vertical free space coupling strategies applying Bragg diffraction can be fabricated to couple the out-of-plane emitted photons into a collecting objective. Non-uniform gratings have been employed in integrated systems, reaching high efficiencies of 75.9% at 1533 nm.[26] In the case of InAs QDs operating at 930 nm, the efficiency of such gratings was simulated to be 76.1%.[27] However, these interfaces are not well developed in the AlGaAs/GaAs system, giving rise to a lack of

possible high detection efficiencies, which are indispensable for advanced quantum optical protocols.

In the present work, a tapered focusing grating coupler consisting of $Al_{0.23}Ga_{0.77}As$ is numerically investigated and optimized for the aforementioned D_2 line of ^{87}Rb atoms at 780 nm. These gratings are developed on a buried oxide with a reflecting gold mirror, both maximizing efficiency and enabling strain transfer to the QDs from a piezoceramic substrate. A schematic depiction of such a grating coupler is shown in Fig. 1. To shed light on their competitiveness, two different buried oxides allowing strain transfer from a substrate are exploited, namely SiO_2 and Al_2O_3.

II. DESIGN OF THE ON-CHIP GRATING

Grating couplers are periodic structures with alternating refractive indices capable of diffracting light from an input waveguide mode into free space by means of Bragg diffraction. The underlying principle thereof lies in the constructive and destructive interference of the incident light field and diffracted light from the interfaces between two alternating materials. The incident mode is diffracted both upward and downward, whereby the latter fraction of intensity is either injected into the substrate or reflected to further contribute to the outcoupled fraction. In our model (cf. Fig. 1), a mode source injects the fundamental transverse electric mode into an AlGaAs waveguide, which is adiabatically tapered to a focusing Bragg grating. The AlGaAs thickness was chosen to be 150 nm, and the GaAs QDs have to be placed at the center of this layer in order to ensure high coupling of the fundamental TE mode. A backside mirror consisting of 2 nm Ti acting as an adhesion layer and 100 nm Au is further implemented to achieve enhanced upward transmission. In between the mirror and the active layer, an oxide layer of either SiO_2 or Al_2O_3 is placed. Although SiO_2 is commonly used and easy to deposit, Al_2O_3 provides better film quality, resulting in higher fabrication yields. It further acts as a passivation layer to stabilize the QDs from surface charge noises.[28] The combination of a backside mirror and a buried oxide is pivotal in order to assure a reasonable strain transfer between a piezoceramic substrate and the photonic nanostructure containing QDs, contrary to free-standing nanostructures.
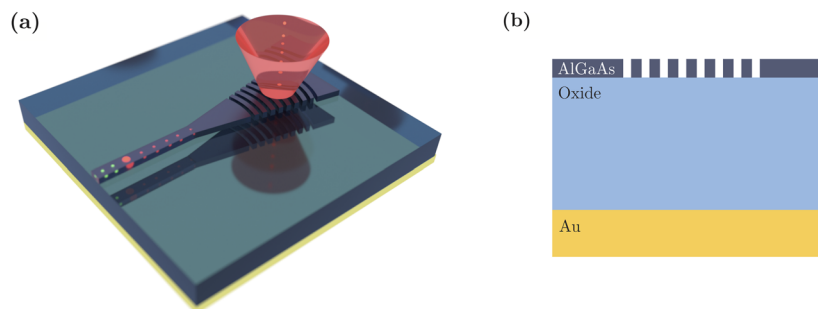
FIG. 1. (a) Perspective view of the simulated structure. Photons emitted from the QD inside a waveguiding section are vertically diffracted by means of Bragg diffraction and collected by collection optics. (b) Schematic cross-section of the model. The grating consists of 150 nm AlGaAs, which is on top of an oxide with simulation-dependent varying thickness and a gold mirror.

The grating period Λ can be tailored to fit the Bragg condition for the corresponding wavelength and can be expressed as[29]

$$\Lambda = \frac{m\lambda}{(n_{\text{eff}} - \sin(\theta))}, \tag{1}$$

in which θ denotes the diffraction angle, n_{eff} is the effective refractive index, and $m \in \mathbb{N}$. In the grating region, the effective refractive index is given as the proportionate sum of the effective indice{s} $n_{\text{eff},1}$ and $n_{\text{eff},2}$ of the grating teeth and the grating trenches, respectively. Therefore, it can be written as

$$n_{\text{eff}} = \text{FF} \cdot n_{\text{eff},1} + (1 - \text{FF}) \cdot n_{\text{eff},2}, \tag{2}$$

where the fill factor FF indicates the ratio between the grating teeth width and the grating period. All simulations were performed with refractive indices at low temperatures since quantum photonic devices are typically operated at cryogenic temperatures. The refractive index is temperature dependent and has to be determined in the first step in order to find suitable parameters that agree with the experiments later on. Accordingly, the refractive index of $Al_{0.23}Ga_{0.77}As$ at $T = 4$ K was estimated to be 3.386 at a wavelength of 780 nm based on Refs. 30–32. The software integrated values for the refractive indices of SiO_2 were used. The fitted value in the wavelength range of 730–830 nm is constant at 1.453 74 due to its weak wavelength dependence. In this case, room temperature values were used since the temperature dependence only affects the refractive index in the third digit after the decimal.[33,34] As for Al_2O_3, measured ellipsometry data were used with $n = 1.620\,84$. Typically, the fundamental transverse electric mode has a higher effective index than the fundamental transverse magnetic mode, which makes grating couplers highly polarization sensitive.[35]

The optical properties of Bragg gratings can be characterized by several metrics. First of all, the grating transmission is a measure determining how much light intensity is diffracted from the grating and transmitted through a frequency-domain profile and power monitor that is placed parallel to the grating surface. The

evolution of the electrical field distribution at larger distances is of huge interest because a homogeneous, Gaussian-like far field distribution improves the coupling efficiency of a single-mode fiber. Another metric quantifying the eligibility of the grating is the grating efficiency. Mathematically, it can be deduced by integrating the collected power flux through the far-field over the corresponding hemispherical cone with azimuthal angle ϕ and half angle θ. Subsequently, this obtained value is normalized by the input power P_{input} at the operation wavelength. The grating efficiency then reads

$$\frac{\int_{\phi=0}^{2\pi} \int_{\theta=0}^{\theta_{NA}} |E(u_x, u_y)|^2 \sin(\theta) d\theta d\phi}{P_{\text{input}}}, \tag{3}$$

in which the electric field E is a function of the direction cosines u_x and u_y.[36]

In the first place, a particle swarm optimization algorithm was applied to obtain a set of parameters where the transmission of the grating was optimized. Based on that solution, several structural parameters, e.g., the grating periodicity, the thickness of the buried oxide, and the fill factor, were swept in order to get a simulation result that features a reasonable trade-off between the aforementioned transmission and a narrow far field distribution. In the following section, the results of the simulations are presented and discussed. The numerical investigations were performed with the software Lumerical finite-difference time domain (FDTD) solutions by ANSYS.

III. RESULTS

At first, a fully etched focusing grating is numerically investigated and optimized to the operation wavelength of 780 nm. For these optimized SiO_2 and Al_2O_3 models, grating periods of 464.8 and 507.7 nm are used, respectively. Both oxide thicknesses are optimized to 150 nm. The acquired data of the transmission spectra for the grating with two dissimilar buried oxide materials are shown
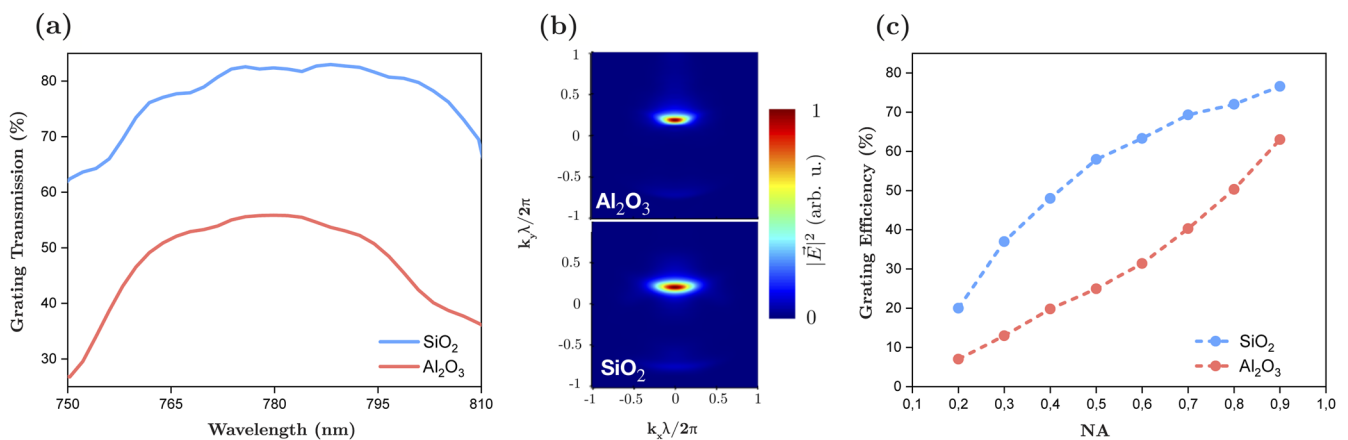
FIG. 2. Simulation results for a fully etched grating at $T = 4$ K. (a) Grating transmission as a function of the wavelength for two different buried oxide materials. The transmission of the SiO_2 buried oxide model is around 25% higher than that of the modeled Al_2O_3 oxide. (b) Far field distributions for both types of grating designs at $\lambda = 780$ nm. (c) Grating efficiency as a function of the NA. A common NA = 0.7 objective yields efficiencies of up to 70% and 40% for Al_2O_3 and SiO_2 buried oxides, respectively.

in Fig. 2(a). Both spectra peak at around 780 nm and are broadband over several tens of nanometers. In the case of SiO_2 oxide, the transmission value reads around 80%, whereas the peak value for the Al_2O_3 grating is limited to around 55%. This major discrepancy can be explained by the differences in refractive indices for both materials. Since the refractive index of Al_2O_3 is higher than that of SiO_2, more light intensity is lost in the vicinity of the substrate. In Fig. 2(b), both far-field distributions are presented. Comparingly, they indicate homogeneous electric field distributions with their maxima slightly shifted from the center. In this regard, back reflections into the waveguide originating from higher order diffractions, which can cause Fabry–Pérot oscillations, are minimized. Such Fabry–Pérot oscillations are usually unwanted because they cause fringes in the spectra. Despite having a lower transmission, the far field in the case of the buried Al_2O_3 is narrower, thus improving the grating efficiency, which is shown in Fig. 2(c). Here, the dependence of the calculated grating efficiencies according to Eq. (3) on the numerical aperture (NA) of an objective is shown. Higher NA corresponds to larger opening angles of the hemispherical far field cone. Therefore, a larger NA results in an elevated grating efficiency since more of the diffracted light can be captured. Using a common objective with NA = 0.7, grating efficiencies of 40% and 70% can be obtained for the Al_2O_3 and SiO_2 buried oxides, respectively.

Multi-step lithography processes facilitate the fabrication of shallow etched nanostructures, i.e., structures in which the trenches are not fully etched. Although it is accompanied by an increase in manufacturing complexity, shallow etching can provide a larger transmission of light through the coupling nanostructures. Figure 3(a) shows the perspective view of a shallow etched focusing grating. In Fig. 3(b), the simulations reveal that the transmission in the case of the shallow etched grating with SiO_2 buried oxide is almost 10% larger than for the fully etched design as presented in Fig. 2(a). On the other hand, the magnitude of the transmission of the shallow etched grating with buried Al_2O_3 oxide is not dramatically changed in comparison to the fully etched grating, although the bandwidth is several nm larger. Exemplarily, the influence of the etch depth on the wavelength dependent transmission is displayed in Fig. 3(c) for the Al_2O_3 containing device. Larger etch depths tend to shift the transmission maxima toward shorter wavelengths with increasing magnitude. This shift can be explained by taking into account Eq. (1). It is visible that deviations from the optimum oxide thicknesses due to, e.g., fabrication imperfections lead to a reduced transmission of the target wavelength. For example, with a fabrication uncertainty of 10 nm, it can be seen that the center of the transmission gets shifted around 10 nm. Though the target wavelength of 780 nm is still in the transmission window, its efficiency is reduced. Since the shallow etching yields an increase in the effective index, the coherent constructive interference condition shifts toward shorter wavelengths for a fixed grating period. However, as shown in Fig. 3(d), the far field pattern for a transmission optimized shallow etched grating is less homogeneous. Interestingly, distinct higher order diffractions are visible for both grating models, yielding a larger loss for coupling into a single-mode fiber due to further scattering. Optimized etch depths were found to be 110 and 140 nm in the cases of the Al_2O_3 and SiO_2 models, respectively.

As was shown in the previous results, light diffracted from uniform gratings suffers from an asymmetric far field distribution, ultimately reducing the fiber coupling efficiency. Gaussian-like electric field profiles that result in a higher mode overlap at a fiber[37,38] or an objective can be achieved by employing non-uniform gratings with spatially varying grating teeth. These apodized gratings were demonstrated to have efficiencies as high as 75.9% at an operation wavelength of 1533 nm for the well-established silicon-on-insulator technology.[26] More recently, an apodized grating design with 76.1% simulated efficiency was used to couple light emitted by a single waveguide integrated QD at a design wavelength of 930 nm into a collection objective.[27]
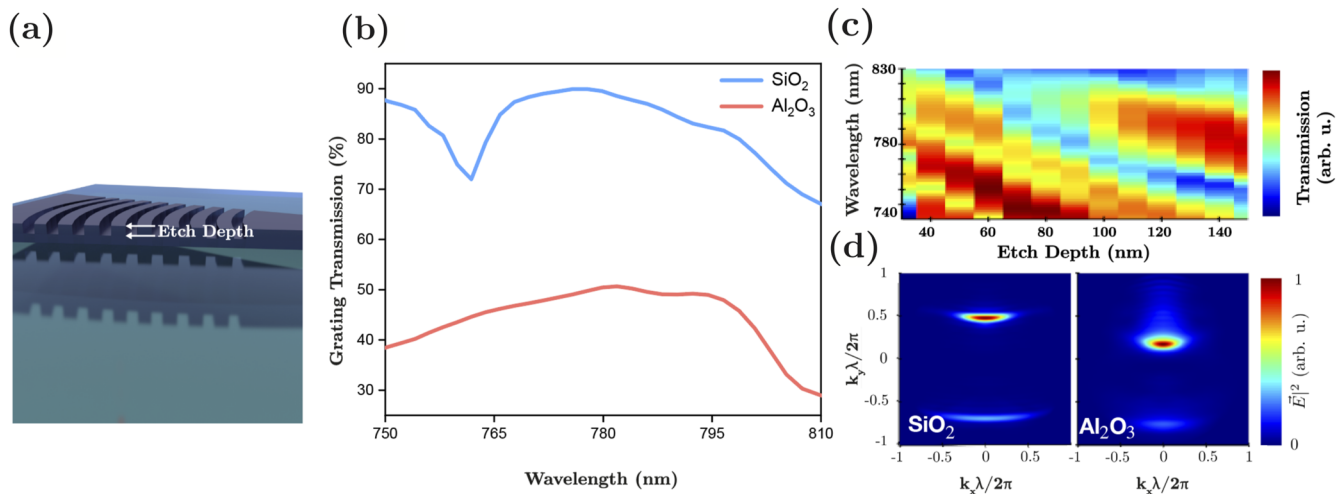
FIG. 3. Simulation results for a shallow etched grating. (a) Perspective view of a shallow etched device. (b) Grating transmission as a function of the wavelength for two different buried oxide materials. The SiO_2 model yields transmissions of up to 90%. (c) Influence of the etch depth of the SiO_2 device on the transmission. (d) Far field distributions for both types of grating designs.

Following this approach, fully etched apodized gratings were implemented and optimized to the target wavelength of 780 nm. Large overlap integral values for the far field profiles and fiber modes have been reported for apodized structures, wherein the fill factors are spatially varying. In contrast to uniform gratings, where the outcoupled light suffers from an exponentially decaying asymmetric field profile, apodized structures diffract light in a distribution resembling a Gaussian.[39] The optimum apodization for the SiO_2 model was evaluated at 0.001 43 with a period of 437.5 nm. The results thereof are presented in Fig. 4. Similar to the uniform grating designs, the upper curve representing the SiO_2 device shows a significantly larger transmission of 80% at the operation wavelength than the lower curve displaying the Al_2O_3 buried oxide grating with 55% transmission in Fig. 4(a).

Notably, the far field pattern, here shown for the SiO_2 grating in Fig. 4(c), shows a more symmetric, Gaussian-like shape than that of the uniform grating structures. Cross-sections in the k_x and k_y directions of the electric field profile are displayed in Figs. 4(d)–4(f), respectively. Orthogonally to the initial propagation direction inside the waveguide-grating device, the field profile was compared to a Gaussian function with an overlap of 98.23%. In the k_y direction, the electric field distribution resembles a Gaussian function with a small side peak yielding an overlap of 86.59%. Multiple higher order
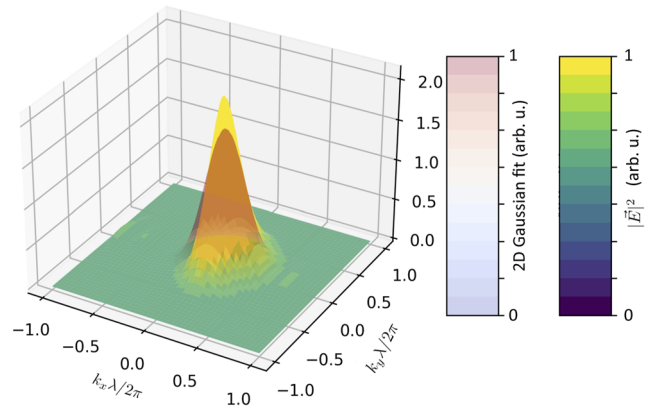

FIG. 5. Graphical visualization of the gathered far field data and a 2D Gaussian fit. An overlap of 83.39% was calculated.

diffractions of small intensity values are visible. The grating efficiencies are shown in Fig. 4(b). Interestingly, the grating efficiency of the focusing grating with SiO_2 oxide yields high values even for low NAs. For example, using a standard 0.3 NA objective results in a grating
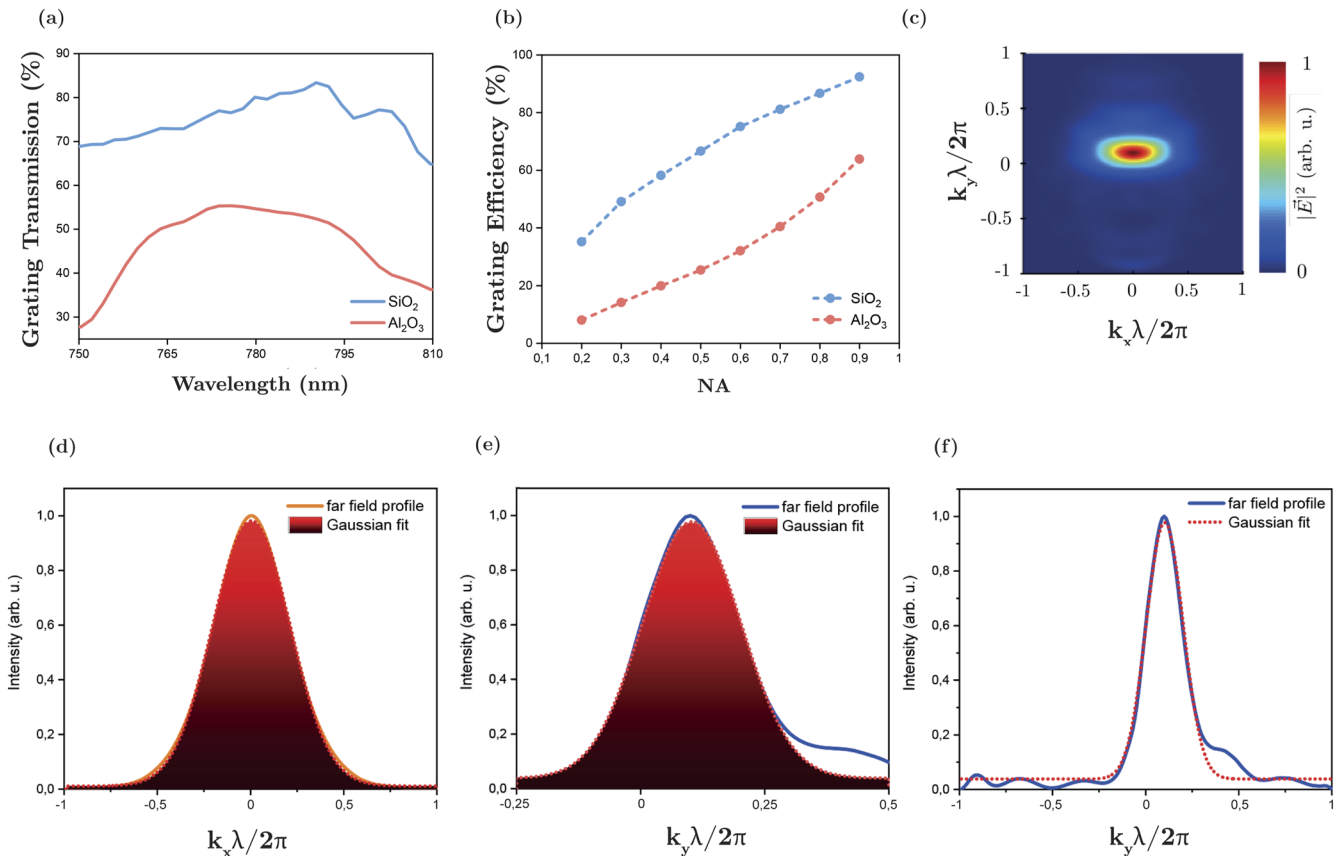
FIG. 4. Simulation results for an apodized grating. (a) Grating transmission as a function of the wavelength for two different buried oxide materials. (b) Grating efficiency as a function of standard numerical apertures. (c) Far field distribution showing a homogeneous electric field pattern. (d) $k_x\lambda/2\pi$ cross-section and Gaussian fit yielding an overlap of 96.23%. (e) $k_y\lambda/2\pi$ cross-section and Gaussian fit yielding an overlap of 86.59%. (f) $k_y\lambda/2\pi$ cross-section showing multiple higher order diffractions.

11 March 2024 08:04:42

TABLE I. Summarized results from the simulation ensembles.

	Fully etched		Shallow etched		Fully etched with apodization	
	Al_2O_3	SiO_2	Al_2O_3	SiO_2	Al_2O_3	SiO_2
Transmission (%)	55	80	50	88	55	80
Efficiency (NA = 0.7) (%)	40	70	$\cdots$	$\cdots$	40	80

efficiency of around 50%. On the other hand, using a high 0.8 NA objective, an efficiency of nearly 90% can be reached.

In order to estimate the fiber coupling efficiency, the electric field distribution was fitted to a 2D Gaussian function, which is shown in Fig. 5. Evaluating the overlap yields a value of 83.39%. The agreement between the far-field pattern and a Gaussian function suggests a high fiber coupling efficiency. On the other hand, the overlap of the far field distributions of the uniform fully etched grating yields a maximum of 74.23%, while the shallow etched design yields 76.75% due to the lack of homogeneity of the electric field distributions. Therefore, this type of apodized grating is beneficial for both free-space propagation and fiber based frameworks with high efficiencies.

IV. CONCLUSIONS

We investigated the properties and theoretical efficiencies of tapered focusing gratings used for coupling light in and out of an AlGaAs waveguide architecture. Different commonly used buried oxide materials for hybrid on-chip strain transfer techniques were compared. FDTD simulations revealed that a uniform, fully etched design yields high grating efficiencies near 80% for high NA objectives while showing moderately homogeneous far field patterns. We further investigated the influence of shallow etched designs and found that the transmission of such gratings can be slightly higher, but au contraire, the electric field distribution of the outcoupled light suffers from a stronger injection into higher order diffraction modes and exhibits a more non-homogeneous far field. Ultimately, this diminishes its applicability in experimental scenarios while also demanding more fabrication effort due to an additional lithography and etching cycle. On evaluating the impact of apodized grating structures, we found that a highly Gaussian-resembling electric field distribution can be accomplished while simultaneously having high grating efficiencies of nearly 90%, showing its strong pertinency for experimental setups involving fiber based networks. Additionally, fabricating apodized gratings does not require further lithography cycles, which demonstrates this type of non-uniform grating to be superior to the aforementioned designs. Although there are powerful alternatives to coupling light from photonic nanostructures, this technique provides high efficiencies while maintaining low adjustment efforts. Overall, the simulations revealed that SiO_2 offers more efficient grating structures when used as a buried oxide instead of Al_2O_3, which we attribute to the lower refractive index of SiO_2. These results suggest the potential for the scalable integration of QDs into chip based photonic networks. An overview of the summarized results are shown in Table 1. In conjunction with strain tuning methods, biexciton and exciton emissions of QD single photon sources can be tuned reversibly without significant deterioration of linewidth and intensity.[22] Beyond the scope of

this, QDs are excellent chip-based sources for generating cluster states[40,41] due to their long spin relaxation times and their ease of integration into selectively transition enhancing photonic nanostructures.[42] Especially photonic crystal waveguides are a feasible platform to control the photon emission of embedded QDs and are particularly suitable for scaling up such systems.[42,43] We emphasize that designing highly efficient coupling methods is a crucial step toward the realization of reliable and sophisticated integrated quantum optical components.

AUTHOR DECLARATIONS

Conflict of Interest

The authors have no conflicts to disclose.

Author Contributions

F.D. conceived the project. M.Z. and E.P.R. supervised the simulations. C.S. designed and performed FDTD simulations. F.B. developed the model for the 2D Gaussian mode overlap calculation. C.M. and J.Y. assisted with the simulations. The manuscript was written by C.S., with the contribution from all co-authors.

Constantin Schmidt: Conceptualization (equal); Investigation (equal); Visualization (equal); Writing – original draft (equal); Writing – review & editing (equal). **Chenxi Ma**: Writing – review & editing (equal). **Frederik Benthin**: Visualization (supporting). **Jingzhong Yang**: Writing – review & editing (supporting). **Eddy P. Rugeramigabo**: Writing – review & editing (supporting). **Michael Zopf**: Project administration (equal); Writing – review & editing (equal). **Fei Ding**: Project administration (equal); Writing – review & editing (equal).

DATA AVAILABILITY

The data that support the findings of this study are available from the corresponding authors upon reasonable request.

REFERENCES

[1] C. Sparrow, E. Martín-López, N. Maraviglia, A. Neville, C. Harrold, J. Carolan, Y. N. Joglekar, T. Hashimoto, N. Matsuda, J. L. O'Brien, D. P. Tew, and A. Laing, "Simulating the vibrational quantum dynamics of molecules using photonics," Nature **557**, 660–667 (2018).

[2] T. Li, G.-J. Yang, and F.-G. Deng, "Heralded quantum repeater for a quantum communication network based on quantum dots embedded in optical microcavities," Phys. Rev. A **93**, 012302 (2016).

[3] I. A. Walmsley, "Quantum optics: Science and technology in a new light," Science **348**, 525–530 (2015).

[4] D. A. Vajner, L. Rickert, T. Gao, K. Kaymazlar, and T. Heindel, "Quantum communication using semiconductor quantum dots," Adv. Quantum Technol. **5**, 2100116 (2022).

[5] W. Wang, Y. Wu, Y. Ma, W. Cai, L. Hu, X. Mu, Y. Xu, Z.-J. Chen, H. Wang, Y. P. Song, H. Yuan, C. L. Zou, L. M. Duan, and L. Sun, "Heisenberg-limited single-mode quantum metrology in a superconducting circuit," Nat. Commun. **10**, 4382 (2019).

[6] A. Majumdar, D. Englund, M. Bajcsy, and J. Vučković, "Nonlinear temporal dynamics of a strongly coupled quantum-dot–cavity system," Phys. Rev. A **85**, 033802 (2012).

[7] D. E. Chang, A. S. Sørensen, E. A. Demler, and M. D. Lukin, "A single-photon transistor using nanoscale surface plasmons," Nat. Phys. **3**, 807–812 (2007).

[8] P. Lombardi, A. P. Ovvyan, S. Pazzagli, G. Mazzamuto, G. Kewes, O. Neitzke, N. Gruhler, O. Benson, W. H. P. Pernice, F. S. Cataliotti, and C. Toninelli, "Photostable molecules on chip: Integrated sources of nonclassical light," ACS Photonics **5**, 126–132 (2018).

[9] N. H. Wan, T.-J. Lu, K. C. Chen, M. P. Walsh, M. E. Trusheim, L. De Santis, E. A. Bersin, I. B. Harris, S. L. Mouradian, I. R. Christen, E. S. Bielejec, and D. Englund, "Large-scale integration of artificial atoms in hybrid photonic circuits," Nature **583**, 226–231 (2020).

[10] C.-Y. Lu and J.-W. Pan, "Quantum-dot single-photon sources for the quantum internet," Nat. Nanotechnol. **16**, 1294–1296 (2021).

[11] L. Schweickert, K. D. Jöns, K. D. Zeuner, S. F. Covre da Silva, H. Huang, T. Lettner, M. Reindl, J. Zichi, R. Trotta, A. Rastelli, and V. Zwiller, "On-demand generation of background-free single photons from a solid-state source," Appl. Phys. Lett. **112**, 093106 (2018).

[12] C. Schimpf, M. Reindl, D. Huber, B. Lehner, S. F. Covre Da Silva, S. Manna, M. Vyvlecka, P. Walther, and A. Rastelli, "Quantum cryptography with highly entangled photons from semiconductor quantum dots," Sci. Adv. **7**(16), 1 (2021).

[13] N. Tomm, A. Javadi, N. O. Antoniadis, D. Najer, M. C. Löbl, A. R. Korsch, R. Schott, S. R. Valentin, A. D. Wieck, A. Ludwig, and R. J. Warburton, "A bright and fast source of coherent single photons," Nat. Nanotechnol. **16**, 399–403 (2021).

[14] C. Hopfmann, W. Nie, N. L. Sharma, C. Weigelt, F. Ding, and O. G. Schmidt, "Maximally entangled and gigahertz-clocked on-demand photon pair source," Phys. Rev. B **103**, 075413 (2021).

[15] L. Zhai, M. C. Löbl, G. N. Nguyen, J. Ritzmann, A. Javadi, C. Spinnler, A. D. Wieck, A. Ludwig, and R. J. Warburton, "Low-noise GaAs quantum dots for quantum photonics," Nat. Commun. **11**, 4745 (2020).

[16] L. Béguin, J.-P. Jahn, J. Wolters, M. Reindl, Y. Huo, R. Trotta, A. Rastelli, F. Ding, O. G. Schmidt, P. Treutlein, and R. J. Warburton, "On-demand semiconductor source of 780-nm single photons with controlled temporal wave packets," Phys. Rev. B **97**, 205304 (2018).

[17] J. Wolters, G. Buser, A. Horsley, L. Béguin, A. Jöckel, J.-P. Jahn, R. J. Warburton, and P. Treutlein, "Simple atomic quantum memory suitable for semiconductor quantum dot single photons," Phys. Rev. Lett. **119**, 060502 (2017).

[18] M. T. Rakher, R. J. Warburton, and P. Treutlein, "Prospects for storage and retrieval of a quantum-dot single photon in an ultracold ^{87}Rb ensemble," Phys. Rev. A **88**, 053834 (2013).

[19] C. Heyn, A. Stemmann, T. Köppen, C. Strelow, T. Kipp, M. Grave, S. Mendach, and W. Hansen, "Highly uniform and strain-free GaAs quantum dots fabricated by filling of self-assembled nanoholes," Appl. Phys. Lett. **94**, 183113 (2009).

[20] R. B. Patel, A. J. Bennett, I. Farrer, C. A. Nicoll, D. A. Ritchie, and A. J. Shields, "Two-photon interference of the emission from electrically tunable remote quantum dots," Nat. Photonics **4**, 632–635 (2010).

[21] Y. Chen, J. Zhang, M. Zopf, K. Jung, Y. Zhang, R. Keil, F. Ding, and O. G. Schmidt, "Wavelength-tunable entangled photons from silicon-integrated III–V quantum dots," Nat. Commun. **7**, 10387 (2016).

[22] L. Tao, W. Wei, Y. Li, W. Ou, T. Wang, C. Wang, J. Zhang, J. Zhang, F. Gan, and X. Ou, "On-chip integration of energy-tunable quantum dot based single-photon sources via strain tuning of GaAs waveguides," ACS Photonics **7**, 2723–2730 (2020).

[23] J. D. Cohen, S. M. Meenehan, and O. Painter, "Optical coupling to nanoscale optomechanical cavities for near quantum-limited motion transduction," Opt. Express **21**, 11227–11236 (2013).

[24] R. S. Daveau, K. C. Balram, T. Pregnolato, J. Liu, E. H. Lee, J. D. Song, V. Verma, R. Mirin, S. W. Nam, L. Midolo, S. Stobbe, K. Srinivasan, and P. Lodahl, "Efficient fiber-coupled single-photon source based on quantum dots in a photonic-crystal waveguide," Optica **4**, 178–184 (2017).

[25] M. Davanço, M. T. Rakher, W. Wegscheider, D. Schuh, A. Badolato, and K. Srinivasan, "Efficient quantum dot single photon extraction into an optical fiber using a nanophotonic directional coupler," Appl. Phys. Lett. **99**, 121101 (2011).

[26] X. Chen, C. Li, C. K. Y. Fung, S. M. G. Lo, and H. K. Tsang, "Apodized waveguide grating couplers for efficient coupling to optical fibers," IEEE Photonics Technol. Lett. **22**, 1156–1158 (2010).

[27] X. Zhou, I. Kulkova, T. Lund-Hansen, S. L. Hansen, P. Lodahl, and L. Midolo, "High-efficiency shallow-etched grating on GaAs membranes for quantum photonic applications," Appl. Phys. Lett. **113**, 251103 (2018).

[28] S. Manna, H. Huang, S. F. C. da Silva, C. Schimpf, M. B. Rota, B. Lehner, M. Reindl, R. Trotta, and A. Rastelli, "Surface passivation and oxide encapsulation to improve optical properties of a single GaAs quantum dot close to the surface," Appl. Surf. Sci. **532**, 147360 (2020).

[29] L. Chrostowski and M. Hochberg, *Silicon Photonics Design: From Devices to Systems* (Cambridge University Press, Cambridge, 2015).

[30] N. Sarkar and S. Ghosh, "The temperature dependence of the band gap shrinkage due to the electron–phonon interaction in $Al_xGa_{1-x}As$," J. Phys.: Condens. Matter **18**, 1687–1694 (2006).

[31] S. Adachi, "GaAs, AlAs, and $Al_xGa_{1-x}As$: Material parameters for use in research and device applications," J. Appl. Phys. **58**, R1–R29 (1985).

[32] S. Gehrsitz, F. K. Reinhart, C. Gourgon, N. Herres, A. Vonlanthen, and H. Sigg, "The refractive index of $Al_xGa_{1-x}As$ below the band gap: Accurate determination and empirical modeling," J. Appl. Phys. **87**, 7825–7837 (2000).

[33] G. Rego, "Temperature dependence of the thermo-optic coefficient of SiO_2 glass," Sensors **23**, 6023 (2023).

[34] J. Gong, R. Dai, Z. Wang, C. Zhang, X. Yuan, and Z. Zhang, "Temperature dependent optical constants for SiO_2 film on Si substrate by ellipsometry," Mater. Res. Express **4**, 085005 (2017).

[35] D. Taillaert, H. Chong, P. Borel, L. Frandsen, R. De La Rue, and R. Baets, "A compact two-dimensional grating coupler used as a polarization splitter," IEEE Photonics Technol. Lett. **15**, 1249–1251 (2003).

[36] H. Huang, S. Manna, C. Schimpf, M. Reindl, X. Yuan, Y. Zhang, S. F. C. da Silva, and A. Rastelli, "Bright single photon emission from quantum dots embedded in a broadband planar optical antenna," Adv. Opt. Mater. **9**, 2001490 (2021).

[37] K. A. Bates, L. Li, R. L. Roncone, and J. J. Burke, "Gaussian beams from variable groove depth grating couplers in planar waveguides," Appl. Opt. **32**, 2112–2116 (1993).

[38] R. Waldhäusl, B. Schnabel, P. Dannberg, E.-B. Kley, A. Bräuer, and W. Karthe, "Efficient coupling into polymer waveguides by gratings," Appl. Opt. **36**, 9383–9390 (1997).

[39] N. H. Lindner and T. Rudolph, "Proposal for pulsed on-demand sources of photonic cluster state strings," Phys. Rev. Lett. **103**, 113602 (2009).

[40] I. Schwartz, D. Cogan, E. R. Schmidgall, Y. Don, L. Gantz, O. Kenneth, N. H. Lindner, and D. Gershoni, "Deterministic generation of a cluster state of entangled photons," Science **354**, 434–437 (2016).

[41] G. Son, S. Han, J. Park, K. Kwon, and K. Yu, "High-efficiency broadband light coupling between optical fibers and photonic integrated circuits," Nanophotonics **7**, 1845–1864 (2018).

[42] M. H. Appel, A. Tiranov, A. Javadi, M. C. Löbl, Y. Wang, S. Scholz, A. D. Wieck, A. Ludwig, R. J. Warburton, and P. Lodahl, "Coherent spin-photon interface with waveguide induced cycling transitions," Phys. Rev. Lett. **126**, 013602 (2021).

[43] K. Tiurev, M. H. Appel, P. L. Mirambell, M. B. Lauritzen, A. Tiranov, P. Lodahl, and A. S. Sørensen, "High-fidelity multiphoton-entangled cluster state with solid-state quantum emitters in photonic nanostructures," Phys. Rev. A **105**, L030601 (2022).